

**Weierstraß-Institut**  
**für Angewandte Analysis und Stochastik**  
**Leibniz-Institut im Forschungsverbund Berlin e. V.**

Preprint

ISSN 0946 – 8633

**Directional reversals and multimode dynamics in  
semiconductor ring lasers**

Antonio Pérez-Serrano<sup>1</sup>, Julien Javaloyes<sup>2</sup>, Salvador Balle<sup>3</sup>

submitted: December 3, 2013

<sup>1</sup> Weierstrass Institute  
Mohrenstr. 39  
10117 Berlin  
Germany  
E-Mail: Antonio.Perez-Serrano@wias-berlin.de

<sup>2</sup> Universitat de les Illes Balears  
Cra. Valldemossa, km 7.5  
07122 Palma de Mallorca  
Spain  
E-Mail: julien.javaloyes@uib.es

<sup>3</sup> Institut Mediterrani d'Estudis Avançats  
C/ Miquel Marquès 21  
07190 Esporles  
Spain  
E-Mail: salvador@imedea.uib-csic.es

No. 1879  
Berlin 2013



---

2010 *Mathematics Subject Classification.* 78A60, 65P30, 65M99, 58J45, 35B32.

2010 *Physics and Astronomy Classification Scheme.* 42.55.Px, 42.55.Sa, 42.60.Mi, 42.65.Pc, 42.65.Sf.

*Key words and phrases.* Semiconductor lasers, traveling wave model (TWM), multimode dynamics, instabilities.

J.J. acknowledges financial support from the Ramon y Cajal fellowship. J.J. and S.B. acknowledge financial support from project RANGER (TEC2012-38864-C03-01) and from the Direcció General de Recerca, Desenvolupament Tecnològic i Innovació de la Conselleria d'Innovació, Interior i Justícia del Govern de les Illes Balears co-funded by the European Union FEDER funds.

Edited by  
Weierstraß-Institut für Angewandte Analysis und Stochastik (WIAS)  
Leibniz-Institut im Forschungsverbund Berlin e. V.  
Mohrenstraße 39  
10117 Berlin  
Germany

Fax: +49 30 20372-303  
E-Mail: [preprint@wias-berlin.de](mailto:preprint@wias-berlin.de)  
World Wide Web: <http://www.wias-berlin.de/>

## Abstract

We investigate the dynamics of longitudinal modes in quantum-well semiconductor ring lasers by means of a spatio-temporal travelling wave model. We report the existence of a novel multimode instability in such a system that provokes a periodic deterministic directional reversal involving jumps between consecutive longitudinal modes. The switching sequence follows the modal frequencies from blue to red, and every modal jump is accompanied by a reversal of the direction of emission. We characterize and analyze such instability via the bifurcation analysis of the full travelling wave model as well as by performing the linear stability analysis of the monochromatic solutions.

## 1 Introduction

Semiconductor Ring Lasers (SRLs) are interesting and promising laser sources from diverse perspectives. From the technological point of view, they do not require cleaved facets to form a resonant cavity, they can be tested on a wafer scale before dicing and they can emit single-mode without the use of Bragg gratings. Therefore they are simpler to fabricate and to integrate in Photonic Integrated Circuits (PICs) [1] than either Fabry-Pérot (FP) or Distributed Feedback (DFB) lasers. From the physical point of view, SRLs are very interesting devices because they show a rich variety of dynamical behaviors including bidirectional continuous wave (Bi-CW) operation [2], intensity Alternate Oscillations (AO) between the counter-propagating electric fields [3], unidirectional (UNI) bistable emission [4], directional multistability [5] and cavity-enhanced Four-Wave Mixing (FWM) [6].

At relatively high pump currents the strong competition for the gain imposes that only one of the two counter-propagating fields can be active, hereby leading to directional bistability. In this case the direction of emission can be switched by optical trigger pulses at ultrafast speeds [7, 8]. Directional bistability has been extensively investigated due to its direct application to perform all-optical processing, because unlike previously proposed optical bistables [9], SRLs meet simultaneously all the stringent requirements for the development of viable integrated functional photonics, such as speed, small footprint, low switching energy and easy read/write mechanism. This feature has been exploited to demonstrate applications such as all-optical memories [10], logic gates [11], flip-flops [12], random bit generators [13, 14] and data processors [15].

In addition, the emission wavelength of a SRL exhibits multistability and can be switched either by optical trigger pulses [16] or by wavelength-selective feedback [17, 12]. The coexistence and nonlinear interaction between directional and spectral domain modes provides rich opportunities for implementing basic logical functionalities, e.g. a 2-bit memory was demonstrated using wavelength/directional multistability between two cavity modes [18].

This variety of dynamical behaviors has been successfully described by means of a Travelling Wave Model (TWM) that incorporates a mesoscopic approximation to the optical response of semiconductor Quantum Well (QW) media valid for time scales longer than 1 ps [19, 20, 21]. Direct integration of the TWM has allowed to successfully explain the main dynamical characteristics of free-running SRLs including lasing direction hysteresis [22] and to highlight the strong impact that residual reflections in the light extraction sections have on the selection of the lasing mode [23]. The TWM has also been used to investigate directional switching [24] and FWM [25] in SRLs subject to optical injection.

In this paper, we present and analyze a novel multimode instability in SRLs that consists of a periodic reversal —on a slow time scale of tens of nanoseconds— of the direction of emission that occurs through jumps between consecutive longitudinal modes. Between reversals, the SRL operates in a single-mode UNI regime, and at each jump the frequency of emission proceeds from blue to red. Although it bears some similarity with the instability reported in [26, 27] for FP lasers, where the emission of the laser passed from the bluest longitudinal mode to the reddest, in our case every modal jump is accompanied by a directional reversal which has important implications. We show that due to the extra degree of freedom that stems from the directional bistability, the threshold for this instability is much lower than it is in FP lasers, which can hinder the performances of SRLs at relatively low bias current. Our theoretical analysis is based on the Linear Stability Analysis (LSA) of the monochromatic solutions of the full spatio-temporal TWM for semiconductor media, which generalizes the method we developed in the past for the simpler two-level atom laser [28]. Our results reveal that, while the mechanism that produces the modal jumps from the bluest toward the reddest frequencies is the same in both FP and SRLs —the asymmetry of the gain spectrum [26, 27], the  $\alpha$ -factor and the so-called Bogatov effect [29] — the directional reversals are energetically preferred in unidirectional SRLs because they allow avoiding FWM effects and only involve mixing between two detuned counter-propagating waves. This result is particularly surprising since the population grating involved in the directional reversal consists of a half-wavelength grating that is strongly washed-out by carrier diffusion.

The paper is organized as follows. In Sec. 2, the theoretical methods used are described, including a summary of the TWM and the methods used to perform its numerical integration and bifurcation analysis. Further technical details on the numerical implementation of the LSA for the TWM in the general case are given in Appendix A. In Sec. 3 we present the multimode instability obtained by numerical integration of the TWM. In order to explain its dynamical origin, an approximate LSA is performed in the Uniform Field Limit (UFL) [30] (see Appendix B for the details) which is compared to the numerical LSA in the general case.

## 2 Theoretical methods

Our analysis of the multilongitudinal mode dynamics in SRLs is based on the direct integration of a TWM [22] as well as on the LSA of its monochromatic solutions, which allow us to perform their bifurcation analysis. In this section we briefly summarize these theoretical tools.

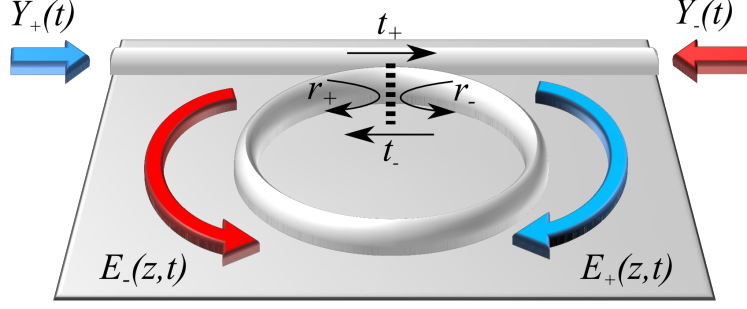


Figure 1: Representation of the semiconductor ring laser. For the sake of simplicity in our model the input/output waveguide is supposed to be transparent and the coupling with the ring cavity described as one point (dashed black line) that imposes the boundary conditions described in Eqs. (6) where  $t_{\pm}$  and  $r_{\pm}$  are the transmission and reflection coefficients for the counter-propagating fields  $E_{+}(z, t)$  and  $E_{-}(z, t)$ .  $Y_{\pm}(t)$  are the injected fields for each direction.

## 2.1 Travelling Wave Model

We summarize here the TWM developed in [22] for the slowly varying amplitudes of the clockwise and counter-clockwise fields,  $E_{\pm}(z, t)$  of a quasi-monochromatic field around an optical carrier frequency  $\omega_0$  and carrier propagation constant  $q_0 = n_0\omega_0/c$ , where  $n_0$  is the effective index of the waveguide for the TE mode. The presence of the counter-propagating fields imposes to the carrier density  $N(z, t)$  a spatial modulation at half the optical wavelength, hence we take

$$N(z, t) = N_0(z, t) + N_{+2}(z, t)e^{2iq_0z} + N_{-2}(z, t)e^{-2iq_0z},$$

where  $N_0(z, t)$  is the local average of the carrier density and  $N_{+2}(z, t) = N_{-2}^*(z, t)$  describes the amplitude of the carrier spatial modulation at half the optical wavelength. The grating variables  $N_{\pm 2}(z, t)$  describe the so-called *short-range* Spatial Hole Burning (SHB), which is due to the standing wave character of the field and the associated variation of the carrier density on the spatial scale of the emission wavelength. Although small, this effect can have a strong influence on the field dynamics and it is the principal ingredient of the transition from BI toward bistable UNI emission in SRLs. It is also capable of provoking a synchronization transition [31, 32], although the effect is more easily seen in cold atom vapors [33] where diffusive effects are mitigated. On the other hand, *long-range* SHB consists of the spatial variation of the carrier density  $N_0(z, t)$  and it is mainly due to the departure from conservative behavior and from the UFL limit of either the point coupler reflection and transmission coefficients in a SRL or to the mirror reflectivities in FP lasers.

Scaling space and time to the ring length  $L_r$  and the ring transit time  $\tau_r = n_g L_r / c$ , where  $n_g$  is the effective group index, our TWM reads

$$(\partial_t \pm \partial_z)E_{\pm} = iP_{\pm} - \alpha_i E_{\pm}, \quad (1)$$

$$\partial_t N_0 = J - R(N_0) - i(P_+ E_+^* + P_- E_-^* - c.c.), \quad (2)$$

$$\partial_t N_{\pm 2} = -[R'(N_0) + \eta]N_{\pm 2} - i(P_{\pm} E_{\mp}^* - E_{\pm} P_{\mp}^*), \quad (3)$$

where  $2\alpha_i$  are the internal losses,  $J$  is the injected current density,  $R(N) = AN + BN^2 + CN^3$  describes carrier recombination, which is modeled with a cubic fitting;  $R' = dR/dN$  is

the effective interband carrier relaxation rate and  $\eta = 4\mathcal{D}q_0^2$  where  $\mathcal{D}$  is the ambipolar diffusion coefficient. In this model, carrier diffusion is included in the evolution of the grating terms  $N_{\pm 2}(z, t)$  only; its effect is negligible on  $N_0(z, t)$  because the characteristic scale of  $N_0(z, t)$  is the cavity length.

The slowly-varying amplitudes of the polarizations of the QW medium,  $P_{\pm}(z, t)$ , are determined from a mesoscopic approximation to the optical response of the semiconductor QW material [19] and computed via a convolution integral [21],

$$P_{\pm}(z, t) = \int_0^{\infty} dt' \{ \chi[t', N_0(z, r)] E_{\pm}(z, r) + \chi_N[t', N_0(z, r)] N_{\pm 2}(z, r) E_{\mp}(z, r) \} + \beta \xi_{\pm}(z, t), \quad (4)$$

where  $r = t - t'$ . The convolution kernel has the form

$$\chi(t', N) = \chi_0 e^{-[\gamma + i(\Omega_G - \omega_0)]t'} \frac{2e^{-i\gamma N t'} - 1 - e^{-i\Omega_T t'}}{t'}, \quad (5)$$

where  $\gamma$  is the polarization decay rate,  $\Omega_G$  is the photon frequency corresponding to the gap and  $\Omega_T$  is the maximum photon frequency absorbed by the QW medium. Also,  $\chi_N = \partial\chi/\partial N$  denotes the variation of  $\chi(t', N)$  with carrier density. For the sake of simplicity we use the convolution kernel (5) instead of the one developed in [34] where the electron-hole tails and the effect of the temperature are included. We also add spontaneous emission of amplitude  $\beta$  by including a Gaussian white noise term  $\xi_{\pm}(z, t)$  of zero mean and correlation  $\langle \xi_{\pm}(z, t) \xi_{\pm}(\hat{z}, \hat{t}) \rangle = \delta(t - \hat{t}) \delta(z - \hat{z})$ .

The TWM defined by Eqs. (1)-(4) has to be closed with the boundary conditions for the ring cavity (see Fig. 1). For the sake of simplicity we consider a an optical carrier frequency that corresponds to a cavity mode and we do not take into account the length and the frequency dependence of the light extraction sections [23], hence the boundary conditions read

$$\begin{aligned} E_+(0, t) &= t_+ E_+(1, t) + r_- E_-(0, t) + Y_+(t), \\ E_-(1, t) &= t_- E_-(0, t) + r_+ E_+(1, t) + Y_-(t), \end{aligned} \quad (6)$$

where  $t_{\pm}$  and  $r_{\pm}$  are the transmission and reflection coefficients at the output coupler for the  $E_{\pm}$  fields respectively.  $Y_{\pm}(t)$  are the external fields injected in each propagation direction respectively, which we assume to be Gaussian pulses of the form

$$Y_{\pm}(t) = \sqrt{I_{\pm}} \exp\left(\frac{-t^2}{4\sigma_{\pm}^2} - i\omega_{\pm} t\right), \quad (7)$$

hence their pulse energy is  $E_p^{\pm} = I_{\pm} \sigma_{\pm} \sqrt{2\pi}$  and their pulse FWHM  $\tau_{\pm} \simeq 2.355 \sigma_{\pm}$ .

## 2.2 Numerical integration

Numerical integration and analysis of the TWM is performed after recasting it into an ensemble of Delayed Algebraic Equations (DAEs) [35] using a spatial discretization of  $N = 401$  points (corresponding to a time step  $\Delta t = 31.2$  fs) with a decimation factor  $D = 25$ ; the convolution

kernels are computed using  $M = 26$  points in the past. The numerical algorithm used to integrate Eqs. (1)-(4) can be found in [36, 37]. Moreover than obtaining shorter simulation times, recasting the TWM to DAEs causes the degrees of freedom of the system decrease considerably, allowing us to perform the LSA of the system of Eqs. (1)-(4) in a similar way as we did in [28] and summarized in Sec. 2.3. Unless otherwise is indicated the parameters used are shown in Table 1.

Table 1: Model parameters

Symbol	Value	Units	Meaning
Waveguide Parameters			
$\lambda_0$	1550	nm	Emission wavelength
$n_g$	3.6	-	Effective group index
$\tau_r$	12.5	ps	Ring transit time
$L_r$	1.04	mm	Length of the ring cavity
$2\alpha_i$	14.4	$\text{cm}^{-1}$	Internal losses
$t_{\pm}$	0.95	-	Transmission coefficients
$r_{\pm}$	$(10 + i5) \times 10^{-5}$	-	Reflection coefficients
Active Material Parameters			
$N_t$	$1 \times 10^{18}$	$\text{cm}^{-3}$	Transparency carrier density
$\mathcal{D}$	11.6	$\text{cm}^2\text{s}^{-1}$	Ambipolar diffusion coeff.
$A$	$1 \times 10^{-8}$	$\text{s}^{-1}$	Recombination coeff.
$B$	$7 \times 10^{-10}$	$\text{cm}^3\text{s}^{-1}$	Recombination coeff.
$C$	$1 \times 10^{-29}$	$\text{cm}^6\text{s}^{-1}$	Recombination coeff.
$2\chi_0$	72	$\text{cm}^{-1}$	Maximum modal gain
$\gamma$	$8 \times 10^{12}$	$\text{rad s}^{-1}$	Polarization decay rate
$\Omega_T$	$9 \times 10^{13}$	$\text{rad s}^{-1}$	Top of the band frequency
$\Omega_G$	$5 \times 10^{12}$	$\text{rad s}^{-1}$	Band-gap frequency
$\beta$	$1 \times 10^{-4}$	-	Spontaneous emission

## 2.3 Bifurcation Analysis

The bifurcation analysis of the TWM is a particularly demanding task because the system of Partial Differential Equations (PDEs) that defines the TWM is hyperbolic, hereby presenting advection. As a consequence, it cannot be recast into an ensemble of sparsely coupled Ordinary Differential Equations (ODEs) by the method of lines [38] which allows the use of software packages like AUTO [39] or DDE-BIFTOOL [40] for performing the numerical bifurcation analysis

of ODEs and Delay Differential Equations (DDEs). Our method is based on the discretized temporal map that advances the solution on time while verifying the Courant-Friedrich-Levy (CFL) condition [41]. It allows us to map the different regimes encountered when varying one or several parameters, hereby providing us with the global dynamical scenario.

This is a two-step process: it requires in the first place finding the monochromatic solutions of the system, and then to perform their LSA as one control parameter is scanned. In our past work [28], the simplicity of the two-level atom description allowed us to find the monochromatic solutions of the system by using a shooting method. However, this procedure cannot be directly applied to the present case due to the nonlinear dependence of the convolution kernel on the carrier density, which defines a highly multidimensional nonlinear problem that can be difficult to solve unless a good guess solution is provided.

### 2.3.1 Monochromatic solutions

Numerically, the monochromatic solutions are represented as a state vector  $\vec{V}$  formed by the  $\mathcal{N}$  (real) values needed to specify all the variables at each spatial point, including past values as required to describe both propagation over the decimated mesh and the convolution kernels that yield the polarizations. In order to find these monochromatic solutions, we start from the trivial off solution and we perform its LSA as described below for different values of the control parameter to be scanned, for instance current density  $J$ . For each value of the parameter, we find the eigenvalues that cross the imaginary axis—if any—and their associated eigenvectors. This parameter value represents the threshold of a lasing branch, and we use the eigenvector as the guess solution to solve the multidimensional nonlinear problem for  $\vec{V}$  using a Newton-Raphson algorithm that converges after a few iterations to a bidirectional solution on the corresponding lasing branch. After the different lasing branches have been determined, it is easy to continue each of them by changing the parameter and solving the multidimensional problem using the previous solution as a guess. After that, the LSA is performed for determining the stability of each branch solution as a function of the parameter.

### 2.3.2 Linear Stability Analysis

The method used to perform the LSA of the monochromatic solutions of the TWM (1)-(4) is based on the fact that the evolution of any state vector  $\vec{V}(t)$  over a time step  $h$  can be written as a temporal map  $\vec{V}(t+h) = \vec{U}(h, \vec{V}(t))$ , where  $\vec{U}(h, \vec{V})$  verifies the CFL condition and cancels numerical dissipation [41]. Considering the perturbations  $\vec{v}$  around a monochromatic solution  $\vec{V}(t)$ , one finds the matrix  $\mathbf{M} = \partial \vec{U} / \partial \vec{V}$  representing the linear operator that governs the time evolution of the perturbations around  $\vec{V}(t)$ . One finally computes the  $\mathcal{N}$  Floquet multipliers  $z_{\mathcal{N}}$  of  $\mathbf{M}$  via a QR decomposition method [42], which determine the eigenvalues as  $\lambda_{\mathcal{N}} = h^{-1} \ln z_{\mathcal{N}}$ . As usual, if none of these computed eigenvalues has a positive real part, then one concludes that this monochromatic solution is stable, and unstable otherwise. The details of the numerical implementation of the LSA can be found in the Appendix A. Please notice that the method also allows finding the associated eigenvectors which will prove important in determining the most unstable directions in phase space.

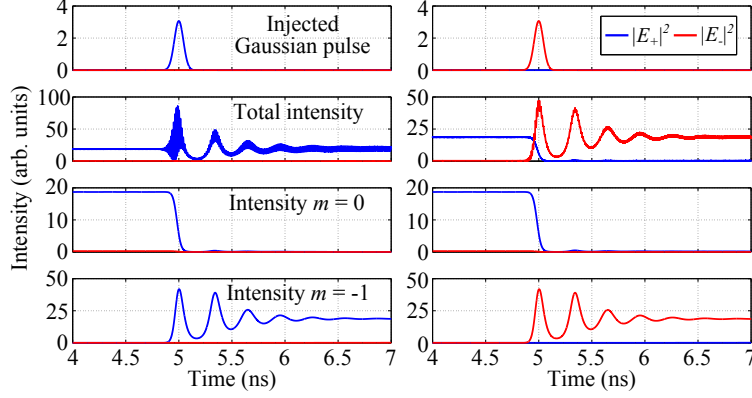


Figure 2: Switching upon injection of a co-propagating (left column) and a counter-propagating (right column) Gaussian pulse with  $I_{\pm} = 3$ ,  $\tau_{\pm} = 100$  ps and  $m = -1$  ( $f = -78$  GHz). From top to bottom, the panels display the Gaussian pulse intensity, the total intensity and the modal intensities for modes  $m = 0$  and  $m = -1$ , obtained filtering the total intensity around each mode. The initial state was at  $m = 0$  ( $\omega = 0$ ),  $J = 2.5$ .

### 3 Results and discussion

For the parameters in Table 1, the SRL shows longitudinal mode bistability between modes  $m = 0$  ( $f = 0$ ) and  $m = -1$  ( $f = -78$  GHz) when it is biased in the UNI regime, for  $J > 2$ . In this situation, and in agreement with experimental results [16, 18], the emission direction and frequency can be switched by optical trigger pulses. Fig. 2 shows how the switching from mode  $m = 0$  to mode  $m = -1$  at  $J = 2.5$  is accomplished by injection of a Gaussian pulse as described in Eq. (7) with  $I_{\pm} = 3$ ,  $\tau_{\pm} = 100$  ps and spectrally centered over mode  $m = -1$  in the co-propagating (left column) and counter-propagating (right column) direction respect to the previous steady state, a clockwise state at  $m = 0$ . In both cases, the modal intensities of  $m = 0$  and  $m = -1$  behave in the same way: mode  $m = 0$  drops to a very low value almost instantaneously, while mode  $m = -1$  switches on through damped relaxation oscillations. The main difference between the two cases is that for the co-propagating case, the beating of the modal amplitudes in the total intensity is much more evident than for the counter-propagating case, which already indicates that switching to a co-propagating mode implies a transient involving more longitudinal modes than when switching to a counter-propagating mode.

Such a situation is encountered over a large current range, and indeed is well reproduced by the LSA of the different monochromatic solutions. The bifurcation diagram for the dominant modes of a SRL with the parameters in Table 1 is shown in Fig. 3. It is seen that mode  $m = 0$  is selected at threshold ( $J_{th} \simeq 1.1$ ) and that it starts to stably lase bidirectionally (Bi-CW) up to  $J \simeq 1.4$ , where a Hopf bifurcation occurs (see Fig. 12 for details) that leads to the AO regime. Finally, a symmetry breaking pitchfork bifurcation takes place after the AO Hopf bifurcation on the Bi-CW solution. This branch will eventually collides with the AO limit cycle as described in [5]; this collision changes the stability of the branch and leads to the unidirectional bistable regime (UNI) for currents  $J \geq 1.65$ . Mode  $m = -1$  presents similar characteristics, but stable lasing on this mode is possible only for currents  $J > 2$ . Above this value of  $J$ , both modes can operate stably in the UNI regime, thus leading to a region of multistability of longitudinal modes

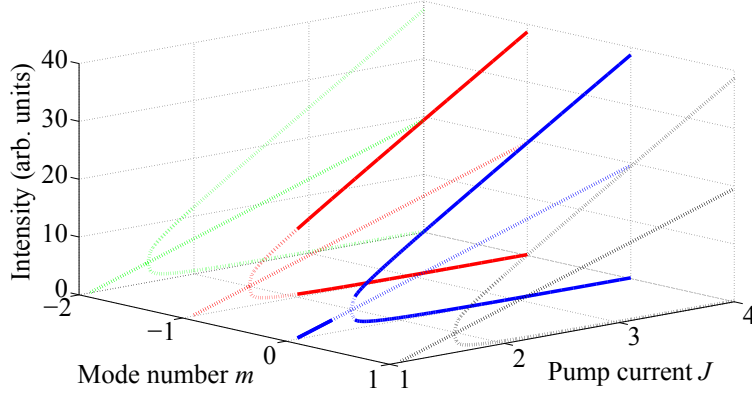


Figure 3: Bifurcation diagrams of the dominant modes of a SRL with the parameters in Table 1. Modes  $m = 0$  and  $m = -1$  share a current region where they are stable in the UNI regime, thus there is longitudinal mode bistability. The other modes are unstable for the explored pump current region.

where the SRL can emit at different wavelengths and propagation directions. On the other hand, the other modes are all unstable for the range of pump values explored.

Interestingly, the range of longitudinal mode multistability is asymmetric with respect to mode  $m = 0$  in spite of having mode  $m = 0$  exactly at the peak gain. This is clearly different from two-level atom case, where the range of multistability was symmetric around the gain peak for mode  $m = 0$  at the gain peak [28]. This is due to the amplitude-phase coupling that occurs in semiconductor materials, that leads to an asymmetry of the gain curve, and the associated Bogatov effect that implies an asymmetric saturation of the gain [29]. In our case,  $\alpha$  is not an input parameter, but it arises through the complex response function of the material; as such, it depends on both operation frequency and carrier density, and in the present case it is  $\alpha \simeq 1.16$ .

For the parameters in Table 1, only two modes are stable up to  $J = 4$ , but the number of stable modes strongly depends on the parameter values, in particular, on the mode spacing as compared to the width of the gain spectrum. Moreover, carrier diffusion  $\mathcal{D}$  plays an important role in the longitudinal mode multistability: it was shown in [28] that FP lasers can exhibit multistability if diffusion is strong enough to wash out the carrier grating, while in SRLs in the UNI regime the carrier grating is always small. Hence, one could expect that multistability in SRLs will disappear for a stronger carrier grating; this can be accomplished by either reducing carrier diffusion or by working at longer wavelengths (i.e. Telecom wavelengths), since both effects reduce  $\eta$  in Eq. 3. In fact, for a diffusion coefficient  $\mathcal{D} = 2.32 \text{ cm}^2 \text{ s}^{-1}$  and the other parameters as in Table 1, the output of the SRL becomes unstable (see Fig. 4), with the direction of emission switching back and forth periodically at a low frequency of a few MHz. Moreover, several modes are involved in the dynamics, but at any given time the laser emits essentially on a single longitudinal mode. Thus this instability does not arise from the locking of different modes giving pulsed operation at the cavity roundtrip time like the Risken-Nummedal-Graham-Haken instability [43], and it is also different from the unstable behavior due to mode competition reported in [44]. Instead, the multimode instability shown in Fig. 4 is similar to the one reported in [26] for FP lasers: there are periodic intensity fluctuations of each mode and the switching sequence follows the modal frequencies from blue to red: when the reddest mode switches off, the sequence restarts from

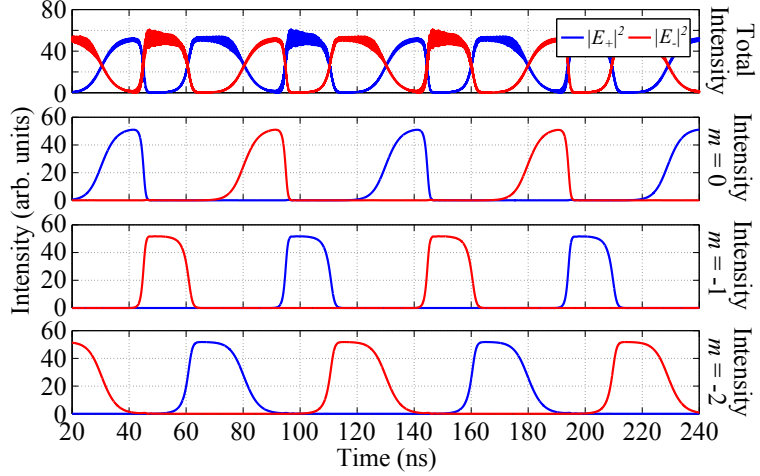


Figure 4: Longitudinal mode switching instability at  $J = 5$ . The period of the oscillation is 100 ns. Parameters as in Table 1 except  $\mathcal{D} = 2.32 \text{ cm}^2 \text{ s}^{-1}$ .

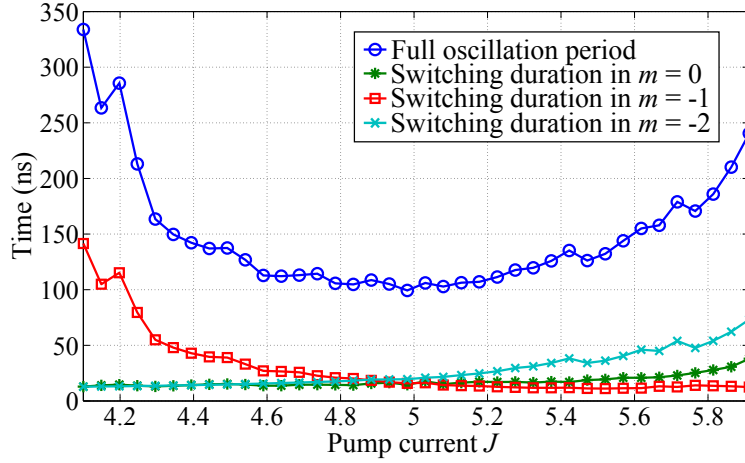


Figure 5: Time characterization of the longitudinal mode switching instability shown in Fig. 4 for different pump current  $J$  values. Parameters as in Table 1 except  $\mathcal{D} = 2.32 \text{ cm}^2 \text{ s}^{-1}$ .

the bluest mode. However in this case each switching has associated a change in the emission direction.

The period of the above dynamics strongly depends on the working point, and also the switching time for the different modes involved. Fig. 5 shows how the period of the oscillation changes as the current  $J$  is increased as well as the duration of the switching in each mode. There is a minimum of the period at  $J \simeq 5$  when the switching duration in the three modes involved is the same. The switching duration for mode  $m = -1$  goes from infinity (when the mode is stable) to finite and decreasing values in the region where the instability is found while the switching duration in modes  $m = 0$  and  $m = -2$  increases monotonically from zero. Finally, when the current is too high ( $J > 6$  for the parameters considered here) the switching becomes incomplete and unsteady multimode emission is obtained. As an example, Fig. 6 shows the output of the SRL for  $J = 6.5$ , that evidences that the emission is mainly in the clockwise direction,

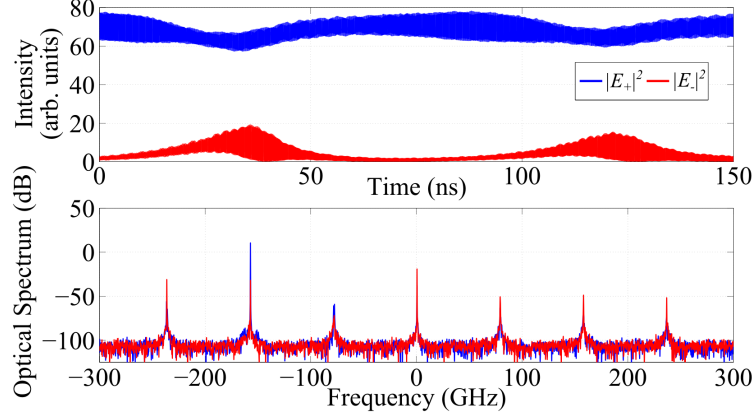


Figure 6: Time trace for  $J = 6.5$  (upper panel) and their optical Spectrum (lower panel). Parameters as in Table 1 except  $\mathcal{D} = 2.32 \text{ cm}^2 \text{ s}^{-1}$ .

although periodic bursts of light in the counter-clockwise direction also occur. Interestingly, the emission in the clockwise direction is dominated by mode  $m = -2$ , while that in the counter-clockwise direction is dominated by mode  $m = 0$ , although in both directions the emission is no longer almost single-mode, thus leading to the fast beat note visible in the direction-resolved traces.

The characteristics of this switching instability change with the spontaneous emission noise. Increasing the noise amplitude  $\beta$ , the behavior shown in Figs. 4 and 5 is conserved, but the duration of the switching and the period of the full oscillation fluctuate. In the absence of spontaneous emission noise ( $\beta = 0$ ), the behavior changes considerably (see Fig. 7), the directional switching and the modal switching are not completed and there are more modes involved in the dynamics due to FWM. The results of Fig. 7 indicate that a small amplitude limit cycle involving modal amplitude oscillation on the slow time scale of 50 ns coexists with the large amplitude limit cycle that consists of multimode directional reversals. This hypothesis is supported by the fact that starting a simulation in the instability shown in Fig. 4 and removing the noise does not lead to the behavior shown in Fig. 7. The behavior shown in Fig. 7 is only achieved starting from a noisy initial condition and performing the simulation with  $\beta = 0$ . From the general point of view of non linear dynamics, one plausible scenario would be that the small amplitude limit cycle and the large amplitude heteroclinic orbit coexist and are separated by an unstable cycle that plays the role of the separatrix in phase space.

In order to get some insight on the origin of this longitudinal mode switching instability and to substantiate our hypothesis, we perform the bifurcation analysis of the monochromatic solutions. Fig. 8 shows the bifurcation diagrams for four modes. In this case mode  $m = 0$  starts to lase Bi-CW but only for a small current range, then a pitchfork bifurcation leads to the UNI regime. In the UNI regime, mode  $m = 0$  eventually becomes unstable at  $J \simeq 2$ , while mode  $m = -1$  becomes stable at  $J \simeq 1.5$  thus leading to a small region of bistability. Mode  $m = -1$  remains stable from this point up to  $J \simeq 4$ , where it becomes unstable again. For  $J > 4$  none of the modes is stable and the instability develops.

The former discussion evidences that the laser becomes unstable, but it does not shed any light

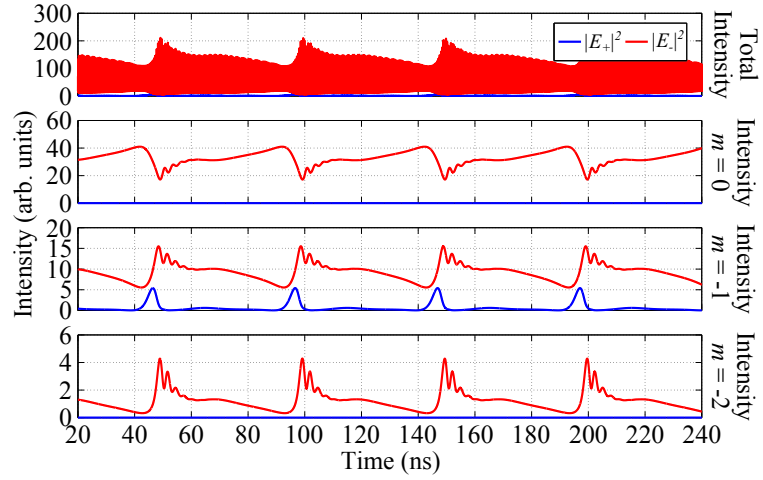


Figure 7: Effect of the absence of spontaneous emission noise in the longitudinal mode switching instability shown in Fig. 4.  $J = 5$ . Parameters as in Table 1 except  $\mathcal{D} = 2.32 \text{ cm}^2 \text{ s}^{-1}$  and  $\beta = 0$ .

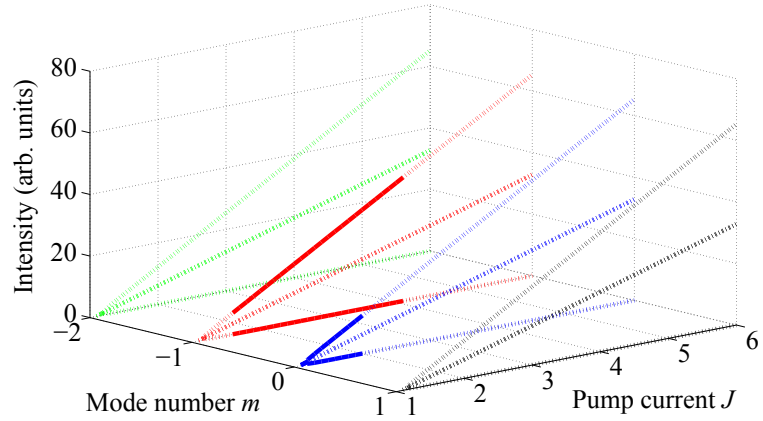


Figure 8: Bifurcation diagrams for four modes for a SRL with the parameters shown in Table 1 except  $\mathcal{D} = 2.32 \text{ cm}^2 \text{ s}^{-1}$ . There is a short region of longitudinal mode bistability between modes  $m = 0$  and  $m = -1$ , however both modes become unstable at different currents and finally there is a multimode instability.

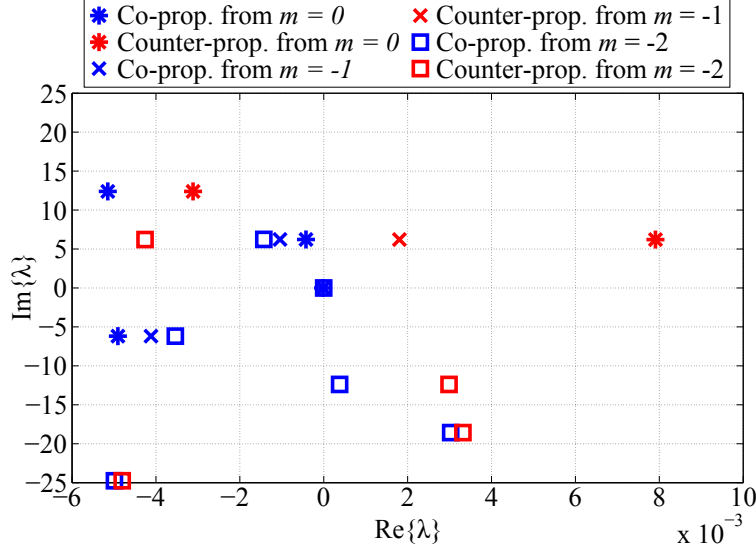


Figure 9: Eigenvalue spectra corresponding to perform the LSA for the steady states for modes  $m = 0$ ,  $m = -1$  and  $m = -2$  at  $J = 5$ . We use the associated eigenvectors in order to find to what direction of emission the eigenvalues correspond.

on why the direction of emission switches in correspondence with the modal jumps. Additional insight can be gained by examining the eigenvalue and eigenvector spectra for the different modes involved in the instability. Fig. 9 shows this eigenvalue spectrum for  $J = 5$ , where we have removed the part corresponding to the complex conjugate eigenvalues for clarity and we have distinguished between co-propagating and counter-propagating solution by using the magnitude of the corresponding eigenvectors into the forward and backward directions. Performing the LSA to a monochromatic UNI solution for  $m = 0$  we find that it is unstable with respect to a counter-propagating solution corresponding to  $m = -1$  ( $m < 0$  for  $\text{Im}\{\lambda\} > 0$ ). We perform the LSA to a monochromatic solution for  $m = -1$  and we find that it is unstable with respect to a counter-propagating solution corresponding to  $m = 0$  (Note that due to the change on the frequency reference frame for performing the LSA, the modal frequencies correspond to  $\text{Im}\{\lambda\} = 0$ ). Finally performing the LSA to a monochromatic solution for  $m = -2$  we find that it is unstable with respect to a counter-propagating solution corresponding to  $m = 1$ , but that there are other unstable eigenvalues, a counter-propagating solution at  $m = 0$  and the co-propagating solution at  $m = 1$ . These results are in agreement with the behavior shown in Fig. 4 and they strongly support the hypothesis of a heteroclinic orbit connecting the laser modes. This is that the eigenvectors are pointing exactly in the direction of the red adjacent modes except for the last mode in the sequence, whose most unstable eigenvector points to the blue mode  $m = 1$  thereby enforcing the periodic behavior of the modal sequence. However, performing the continuation of such heteroclinic connection with a fully spatially resolved TWM would represent a tremendous technical challenge.

The prevalence of counter-propagating perturbations over co-propagating disturbances may seem quite surprising, because counter-propagating waves generate a carrier grating that does not exist for co-propagating waves, hence it may appear that diffusion should have a stronger impact on the former. The physical origin for this fact can be further elucidated by considering

the ideal case of a pure SRL in the UFL, i.e.  $r_{\pm} = 0$  and  $t_{\pm} = 1$ . In this case, it is possible to analytically perform the LSA of the monochromatic solutions similarly to [45] (see Appendix B). Assuming unidirectional operation on a given mode,  $m = s$ , the monochromatic solution—characterized by  $E_+^s \neq 0$ ,  $P_+^s \neq 0$ ,  $N_0^s \neq 0$  and  $E_-^s = P_-^s = N_{\pm 2}^s = 0$ —can be determined as detailed in Appendix B. Here the UFL allows simplifying the spatial dependence of the problem, which reduces to a phase factor  $e^{ik_s z}$  in the field and polarization.

Interestingly, the LSA of the perturbations around such a unidirectional solution decouples counter-propagating from co-propagating perturbations (see Appendix B for the derivation). In the reference frame of the clock-wise UNI lasing solution, counter-propagating perturbations are governed by (38)-(40),

$$\partial_t e_- - \partial_z e_- = -\alpha_i e_- + ip_-, \quad (8)$$

$$\partial_t n_{-2} = -(R'(N_0^s) + \eta)n_{-2} - i(p_- E_+^{s*} - e_- P_+^{s*}), \quad (9)$$

and

$$p_- = \int_0^\infty dt' e^{i\omega_s t'} [\chi(t', N_0^s) e_-(z, t - t') + \partial_N \chi(t', N_0^s) n_{-2}(z, t - t') E_+^s]. \quad (10)$$

Co-propagating perturbations, instead, are ruled by (53)-(55),

$$\partial_t e_+ + \partial_z e_+ = (i\omega_s - ik_s - \alpha_i) e_+ + ip_+, \quad (11)$$

$$\partial_t n_0 = -R'(N_0^s) n_0 - i(P_+^s e_+^* + p_+ E_+^{s*} - c.c.), \quad (12)$$

and

$$p_+ = \int_0^\infty dt' e^{i\omega_s t'} [\chi(t', N_0^s) e_+(z, t - t') + \partial_N \chi(t', N_0^s) n_0(z, t - t') E_+^s]. \quad (13)$$

There are remarkable differences between the two sets of equations. For co-propagating disturbances, the linearized equations describe the generalized multimode relaxation oscillations in a multimode system and they involve slowly spatially evolving carrier pulsation at a spatial frequency equal to  $2\pi m/L_r$  with  $m = 0, \pm 1, \pm 2, \dots$ . As discussed in Appendix B, this imposes that perturbations  $\ell$  modes above  $s$  are coupled to perturbations  $\ell$  modes below  $s$  by carrier-mediated FWM. The reason is that two optical modes, say  $s$  and  $s - \ell$  create a modulation wave in the carrier density at frequency  $\ell$  that is coupled back into the optical field through the active medium polarization in order to generate an additional side mode at frequency  $s + \ell$ .

Instead, the (linearized) evolution of counter-propagating disturbances does not depend on perturbations in the total carrier density  $N_0$  but only on the amplitude of a half wavelength carrier grating mediated through the variable  $N_2$ . The equation for the carrier grating amplitude has a source term such that two counter-propagating plane waves at different frequencies create a population grating that is going to slide along the cavity at a speed given by the frequency difference between the two modes [31, 32]. This sliding grating does not generate new spatial or temporal frequencies for the field through its interaction with the active medium.

As a consequence, counter-propagating perturbations can grow more easily than co-propagating perturbations because for the latter the interaction is mediated by a carrier density wave that imposes that the energy of the perturbation has to be shared among two different modes which in

addition have to maintain a precise phase relation. In other words, creating a carrier grating that slides across the cavity at a given speed is energetically favourable as compared to generating an equivalent pulsation in the carrier density.

Finally, it is worth remarking that, even in the case of an ideal SRL, the eigenvalue equations that result for both co-propagating and counter-propagating solutions are strongly nonlinear. However, simplified eigenvalue equations can be obtained by noting that, for a given mode  $m = \ell$  (with respect to the UNI lasing solution), the eigenvalue must be close to the modal frequency.

In this case, the eigenvalue equation for counter-propagating perturbations becomes a second order polynomial for  $\lambda' = \lambda + 2i\pi\ell$ ,

$$\lambda' = i(\tilde{\chi}_\ell - \tilde{\chi}_s) + \frac{\partial_N \tilde{\chi}_\ell (\tilde{\chi}_\ell - \tilde{\chi}_s^*) |E_+^s|^2}{R'(N_0^s) + \eta + i\partial_N \tilde{\chi}_\ell |E_+^s|^2 + \lambda' - 2i\pi\ell}, \quad (14)$$

where  $\tilde{\chi}_\ell$ ,  $\partial_N \tilde{\chi}_\ell$  and  $\tilde{\chi}_s$  can be found in the Appendix B. Most of the physics of this instability can be understood by inspecting Eq. 14. The first term on the right hand side (RHS) correspond to the gain difference between modes. Since one operate initially at the gain peak, this difference is negative thereby ensuring stable operation with respect to side mode perturbations. The second term in the RHS is the one responsible for the asymmetric modal switching. The numerator contains the differential gain  $\partial_N \tilde{\chi}_n$  which contains the so-called  $\alpha$ -factor while the denominator also contains a complex response that consists of the balance between the modal separation  $2i\pi\ell$ . Clearly, an instability can be promoted for  $\ell < 0$  and inhibited for  $\ell > 0$ . Notice also in this complex denominator the presence of the half-wavelength diffusion factor  $\eta$  which makes this “Two-Wave-Mixing” term small.

In the same way, for a co-propagating perturbation one has to take into account the perturbation in the mode of interest and the perturbation of the mode that it is created by the beating with the monochromatic state [45]. Finally, a fourth order polynomial for the eigenvalue  $\lambda'$  is obtained,

$$\begin{aligned} & \left[ \lambda' - i(\tilde{\chi}_{-\ell} - \tilde{\chi}_s) - \frac{\partial_N \tilde{\chi}_{-\ell} (\tilde{\chi}_{-\ell} - \tilde{\chi}_s^*) |E_+^s|^2}{\lambda' + Y_\ell} \right] \\ & \times \left[ \lambda' + i(\tilde{\chi}_\ell^* - \tilde{\chi}_s^*) - \frac{\partial_N \tilde{\chi}_\ell^* (\tilde{\chi}_\ell^* - \tilde{\chi}_s^*) |E_+^s|^2}{\lambda' + Y_\ell} \right] \\ & - \frac{\partial_N \tilde{\chi}_{-\ell} \partial_N \tilde{\chi}_\ell^* (\tilde{\chi}_\ell^* - \tilde{\chi}_s^*) (\tilde{\chi}_{-\ell} - \tilde{\chi}_s^*) |E_+^s|^4}{(\lambda' + Y_\ell)^2} = 0, \end{aligned} \quad (15)$$

where  $Y_\ell = 2i\pi\ell + R'(N_0^s) - i(\partial_N \tilde{\chi}_\ell^* - \partial_N \tilde{\chi}_{-\ell}) |E_+^s|^2$ . Although Eq. (15) is more involved than Eq. (14), we notice that the first term is composed by the product of two terms similar to Eq. (14).

Fig. 10 show the eigenvalues  $\lambda$  obtained from Eqs. (14) and (15). Comparing Fig. 10 with Fig. 9, we can see that the unstable values are recovered, however there are some differences that come from the assumptions used in the derivation of Eqs. (14) and (15) but the good qualitative agreement makes such approximate analytical expression useful to understand the underlying mechanism of the modal instability. From an extensive parameter study, we found that the instability with respect to co-propagating solution, like the one studied in [26] is always

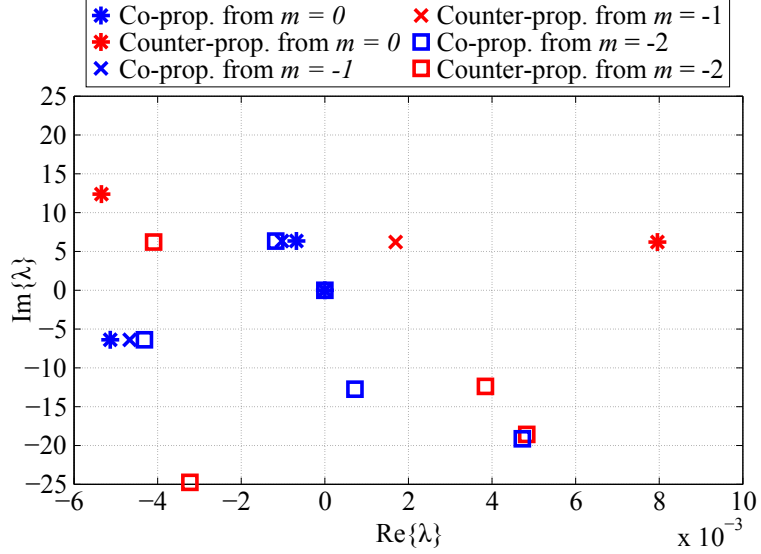


Figure 10: Eigenvalue spectra corresponding to perform the LSA for the steady states for modes  $m = 0$ ,  $m = -1$  and  $m = -2$  at  $J = 5$ . We use the associated eigenvectors in order to find to what direction of emission the eigenvalues correspond.

found for parameters values for which the system already became unstable with respect to directional reversals. This suggests that this modal instability mechanism should be the one dominantly observed experimentally.

## 4 Conclusions

We have investigated theoretically and numerically the multimode dynamics in SRLs by performing the bifurcation analysis of a spatio-temporal TWM with the gain of a semiconductor QW [21]. Our bifurcation analysis extend and generalize the results obtained in [28] for the case of a two-level atom active medium. Our investigation on the longitudinal mode multistability in SRLs has led us to find a novel multimode instability that leads to a dynamical regime where the lasing frequency jumps periodically from one mode to the next. The jumping sequence proceeds, at low frequency, from the bluest to the reddest part of the spectrum and each modal jump is accompanied by a directional reversal. We have identified the modal instability mechanism to be of a similar nature to the one found in [26] which consists of the interplay between the carrier beatings, the asymmetry of the semiconductor gain curve and the  $\alpha$ -factor. However this behavior is found here for much lower bias current due to the extra degree of freedom brought by the directional bistability of the SRLs. We have also found that the spontaneous emission noise plays a crucial role in the mechanism inducing the directional and modal switching. In the absence of spontaneous emission the switching is not achieved, the system only is capable of showing multimode dynamics induced by FWM. This supports the idea of a low amplitude limit cycle that coexists with a large amplitude heteroclinic connection between the monomode solutions. This is not a noise-induced instability, which is against the concept of deterministic bifurcation and cannot be explained by our LSA. Although we were not able to perform a nu-

merical continuation of such heteroclinic connection, such a hypothesis was supported by the analysis of the most unstable eigenvectors around the monomode solutions. Finally, we gave quasi-quantitatively correct approximations to the eigenvalues that defines the boundary of the instable regions which allowed us to contrast the instability threshold for co-propagating and contra-propagating perturbations. Since this directional instability seems to appear always before the co-propagating one in ring lasers, we believe its observation to be possible, especially in long wavelength SRLs. At last, this analysis demonstrates that even the off modes that do not participate in the dynamics can strongly influence the LSA of the lasing modes. For instance a two-mode rate equation model that would consider a strong and a weak mode would be essentially incorrect, unless the two modes correspond to opposite lasing directions. In the case of a strongly multimode regime that consists of  $N$  modes, one that would follow multimode rate equation approach would need at least  $N/2$  mode on each side of the spectrum in order to correctly assess the dynamics.

## A Numerical bifurcation analysis

### A.1 Monochromatic solutions

In our past work [28] the simplicity of the two-level atom description allowed us to find the monochromatic solutions of the system by using a shooting method for the electric fields fulfilling the boundary conditions, while solving a linear system of equations for the material variables in each point. However, finding the monochromatic solutions for the TWM described by Eqs. (1)-(4) can not be done in the same way, because the complexity of the system has increased due to the nonlinearity of the QW response, involving a convolution, and the use of DAEs, thus we are dealing with a highly multidimensional nonlinear problem that can be difficult to solve unless a good guess solution is provided. So we use as described in Sec. 2.3 the eigenvalues obtained from performing the LSA of the off solution as a guess for a Newton-Raphson solver obtaining the monochromatic solutions

Using this procedure allows us to construct bifurcation diagrams like the one shown in Fig. 11 for mode  $m = 0$  corresponding to parameter set shown in Table 1. One can see that the complete L-I curve is recovered [2]. The SRL starts to lase bidirectionally (Bi-CW), then there is an onset of a Hopf bifurcation (see Fig. 12 for details) that leads to the AO regime, and finally the pitchfork bifurcation that takes place inside the AO regime changes its stability and leads to the UNI regime.

Fig. 11 is completely equivalent to Fig. 2 (c) in [46] which was obtained from the bifurcation analysis of a reduced two-mode model for single-longitudinal mode SRLs. In our case the linewidth enhancement factor  $\alpha_H = 1.16$  and we can think that  $\phi_k$  comes mainly from the complex reflection coefficient  $r_{\pm}$ , then  $\phi_k = 1.37$  rad. Our analysis is in agreement with the one performed in [46] in the case of single-mode operation and in the UFL.

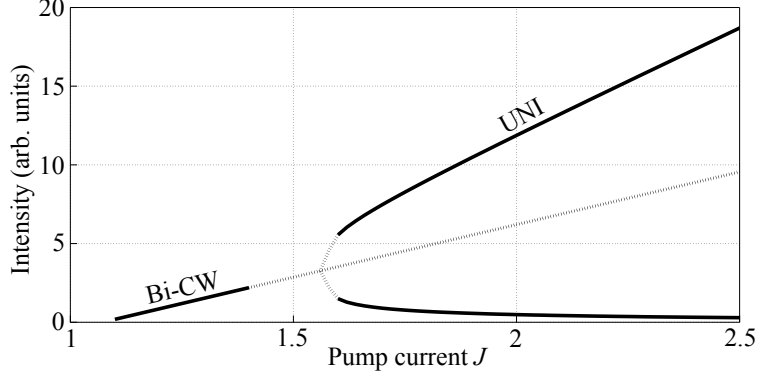


Figure 11: Bifurcation diagram of the mode  $m = 0$  for the parameter set from Table 1. The solid (dotted) black lines indicate stable (unstable) solutions for the branches Bi-CW and UNI. The unstable region around  $J = 1.5$  corresponds to the AO regime.

## A.2 Linear stability analysis

The method used to perform the LSA of the system of Eqs. (1)-(4) is based in the fact that the TWM is written in the time domain. This allow to use the temporal map  $\vec{V}_{j+1} = \vec{U}(h, \vec{V}_j)$  formed by the equations that are used to perform the numerical integration [36]. The temporal map advances the state vector  $\vec{V}$  a time step  $h$  while verifying the CFL condition and canceling numerical dissipation [41].

Considering all possible perturbations of  $\vec{V}$ , one finds the matrix  $\mathbf{M} = \partial\vec{U}/\partial\vec{V}$  representing the linear operator governing the time evolution for the perturbations around one given monochromatic solution:  $E_{\pm}^{st}(z, \Delta t_M)$ ,  $P_{\pm}^{st}(z, \Delta t_D)$ ,  $N_0^{st}(z)$  and  $N_{\pm 2}^{st}(z)$ , where  $\Delta t_M$  and  $\Delta t_D$  represent the time intervals associated to the convolution and the decimation factor respectively.

Numerically, we separate the problem in real and imaginary parts, then our system has a number of independent variables  $\mathcal{N} = K(4M + 3) + 4D(K - 2) + 4(D + 1)$  where  $K = (N - 1)/D + 1$ . In our case  $\mathcal{N} = 3423$ . Where we have taken into account that the carrier density is almost constant in the time span of the convolution kernel calculation (over a few hundred fs) that allow us to perform the approximation  $N_0(z, r) = N_0(z, t)$  and  $N_{\pm 2}(z, r) = N_{\pm 2}(z, t)$  in Eq. (4). To obtain the evolution operator  $\mathbf{M}$ , a  $\mathcal{N} \times \mathcal{N}$  matrix, one calculates each row by introducing a perturbation, i.e. one of the  $\mathcal{N}$  variables is set to 1 whereas the others are zero. Then this state is evolved over one time step according to the numerical algorithm in [36] and taking into account the monochromatic solutions previously calculated. This process is repeated for all variables, obtaining  $\mathbf{M}$ . One finally computes the  $\mathcal{N}$  Floquet multipliers  $z_{\mathcal{N}}$  of  $\mathbf{M}$  via a QR decomposition method, which determine the eigenvalues as  $\lambda_{\mathcal{N}} = h^{-1} \ln z_{\mathcal{N}}$ . As usual if one of these computed eigenvalues has a positive real part, then one concludes that this monochromatic solution is unstable. If none of them has a positive real part, then the monochromatic solution is stable.

Due to the separation of the variables in real and imaginary parts, we obtain two eigenvalue spectra as shown in Fig. 12 (a), one corresponding to the gain curve and the other to their complex conjugate. It can be seen the typical gain asymmetry characteristic of the QW material.

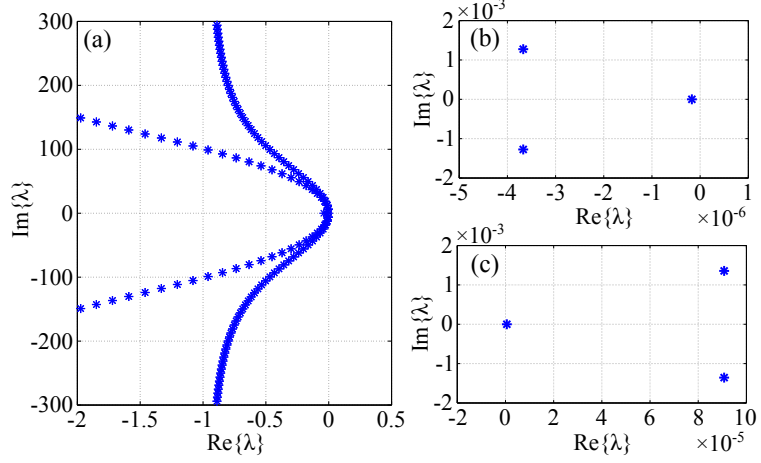


Figure 12: Eigenvalue spectra corresponding to Fig. 11 at  $J = 1.3$  (a) and (b), and  $J = 1.4$  (c). (b) and (c) Onset of the Hopf bifurcation by the crossing of the  $\text{Im}\{\lambda\}$  axis of two complex conjugate eigenvalues. The other eigenvalue shown corresponds to the phase invariance.

We notice that in order of being as more accurate possible in the calculation of the eigenvalues, we perform a change of the frequency reference frame in the lasing solutions, that explains why the maximum of the gain curve is at  $\text{Im}\{\lambda\} = 0$ . It has also to be noticed that using this approach for computing the stability of a monochromatic solution different from the off solution, we obtain a zero eigenvalue corresponding to the phase invariance of the system. This situation is shown in Fig. 12 (b) and (c) where the eigenvalues corresponding to the change of stability of the Bi-CW branch in Fig. 11 are shown. One can see how a pair of complex conjugate eigenvalues cross the  $\text{Im}\{\lambda\}$  axis indicating the onset of the Hopf bifurcation that leads to the AO regime, and the eigenvalue corresponding to the phase invariance, the so-called Goldstone mode. Following this procedure, we can construct the bifurcation diagrams for the dominant modes of a SRL with the parameters in Table 1 shown in Fig. 3.

## B Analytical LSA for an ideal SRL

An ideal SRL is characterized by having no reflection at the output coupler, which in addition provides a lossless cavity. In this system, the boundary conditions (in the absence of injected fields) simply read

$$E_{\pm}(0, t) = E_{\pm}(1, t), \quad (16)$$

where the optical carrier frequency has been taken as that of the mode closest to the gain peak. In these case, the UFL applies and it is possible to perform the LSA analitically.

## B.1 Monochromatic solutions

In order to perform the LSA analytically, the first step is to find the monochromatic solutions of Eqs. (1)-(4). These have the form

$$E_{\pm}(z, t) = E_{\pm}^s e^{\pm i k_s z - i \omega_s t}, \quad (17)$$

$$P_{\pm}(z, t) = P_{\pm}^s e^{\pm i k_s z - i \omega_s t}, \quad (18)$$

$$N_0(z, t) = N_0^s, \quad (19)$$

$$N_{\pm 2}(z, t) = N_{\pm 2}^s e^{\pm 2 i k_s z}, \quad (20)$$

where  $k_s = 2\pi s$  is the wavevector of the monochromatic solution (or mode)  $m = s$ .  $E_{\pm}^s$ ,  $P_{\pm}^s$ ,  $N_0^s$  and  $N_{\pm 2}^s$  define a monochromatic solution that oscillates at angular frequency  $\omega_s$ , and they are given by

$$(i k_s - i \omega_s) E_{\pm}^s = i P_{\pm}^s - \alpha_i E_{\pm}^s, \quad (21)$$

$$P_{\pm}^s = \tilde{\chi}_s E_{\pm}^s + \partial_N \tilde{\chi}_s E_{\mp}^s N_{\pm 2}^s, \quad (22)$$

$$R(N_0^s) - J = -i(E_+^{s*} P_+^s + E_-^{s*} P_-^s - c.c.), \quad (23)$$

$$N_{\pm 2}^s = -i \frac{P_{\pm}^s E_{\mp}^{s*} - E_{\pm}^s P_{\mp}^{s*}}{R'(N_0^s) + \eta}, \quad (24)$$

where

$$\tilde{\chi}_s = \int_0^{\infty} \chi(t', N_0^s) e^{i \omega_s t'} dt', \quad (25)$$

$$\partial_N \tilde{\chi}_s = \int_0^{\infty} \chi_N(t', N_0^s) e^{i \omega_s t'} dt'. \quad (26)$$

Besides the trivial solution  $E_{\pm}^s = 0 = P_{\pm}^s = N_{\pm 2}^s$  and  $J = R(N_0^s)$ , the system admits both bidirectional solutions and unidirectional solutions. The former are difficult to determine analytically, and in addition it has been proven that they are unconditionally unstable [47, 48]. Unidirectional solutions in the clockwise direction are of the form  $E_-^s = P_-^s = N_{\pm 2}^s = 0$ , with  $E_+^s \neq 0$ ,  $P_+^s \neq 0$ ,  $N_0^s \neq 0$  and  $\omega_s$  given by

$$i k_s - i \omega_s = i \tilde{\chi}(\omega_s, N_0^s) - \alpha_i, \quad (27)$$

and

$$|E_+^s|^2 = \frac{J_{th} - J}{2 \text{Im}\{\tilde{\chi}_s\}}, \quad P_+^s = \tilde{\chi}_s E_+^s, \quad J_{th} = R(N_0^s). \quad (28)$$

Obviously, an equivalent unidirectional solution exists that propagates in the opposite direction, which is simply obtained by exchanging the signs in the solution labels.

## B.2 Perturbation analysis of UNI solutions

We consider the monochromatic unidirectional solution corresponding to mode  $m = s$ , that propagates in the clockwise direction, i. e.,  $E_-^s = P_-^s = N_{\pm 2}^s = 0$ ,  $E_+^s \neq 0$ ,  $P_+^s \neq 0$ ,  $N_0^s \neq 0$

and  $\omega_s$  determined by Eqs. (27)-(28). We disturb this solution with space and time dependent perturbations  $e_{\pm}(z, t)$ ,  $p_{\pm}(z, t)$ ,  $n_0(z, t)$  and  $n_{\pm 2}(z, t)$ , with  $n_{-2} = n_{+2}^*$  and  $n_0$  real. We introduce

$$E_{\pm}(z, t) = E_{\pm}^s e^{\pm i k_s z - i \omega_s t} + e_{\pm}(z, t), \quad (29)$$

$$P_{\pm}(z, t) = P_{\pm}^s e^{\pm i k_s z - i \omega_s t} + p_{\pm}(z, t), \quad (30)$$

$$N_0(z, t) = N_0^s + n_0(z, t), \quad (31)$$

$$N_{\pm 2}(z, t) = N_{\pm 2}^s e^{\pm 2 i k_s z} + n_{\pm 2}(z, t), \quad (32)$$

in Eqs. (1)-(4) and linearizing around the UNI solution leads to

$$\partial_t e_{\pm} \pm \partial_z e_{\pm} = i p_{\pm} - \alpha_i e_{\pm}, \quad (33)$$

$$\partial_t n_0 = -R'(N_0^s) n_0 - i(P_+^s e^{i\Phi_s(z,t)} e_+^* + p_+ E_+^{s*} e^{-i\Phi_s(z,t)} - c.c.), \quad (34)$$

$$\partial_t n_{-2} = -[R'(N_0^s) + \eta] n_{-2} - i(p_- E_+^{s*} - e_- P_+^{s*}) e^{-i\Phi_s(z,t)}, \quad (35)$$

$$p_+(z, t) = \int_0^{\infty} [\chi(t', N_0^s) e_+(z, r) + \chi_N(t', N_0^s) E_+^s n_0(z, r) e^{i\Phi_s(z,r)}]_{r=t-t'} dt' \quad (36)$$

$$p_-(z, t) = \int_0^{\infty} [\chi(t', N_0^s) e_-(z, r) + \chi_N(t', N_0^s) E_+^s n_{-2}(z, r) e^{i\Phi_s(z,r)}]_{r=t-t'} dt' \quad (37)$$

where  $\Phi_s(z, t) = k_s z - \omega_s t$ . Perturbations associated with opposite propagation directions decouple from each other, which allows for a separate analysis.

### B.2.1 Counter-propagating perturbation

Propagations that propagate in the counter-clockwise direction evolve (in the linearized regime) according to

$$\partial_t e_- - \partial_z e_- = i p_- - \alpha_i e_-, \quad (38)$$

$$\partial_t n_{-2} = -[R'(N_0^s) + \eta] n_{-2} - i(p_- E_+^{s*} - e_- P_+^{s*}) e^{-i\Phi_s(z,t)}, \quad (39)$$

$$p_-(z, t) = \int_0^{\infty} [\chi(t', N_0^s) e_-(z, r) + \chi_N(t', N_0^s) E_+^s n_{-2}(z, r) e^{i\Phi_s(z,r)}]_{r=t-t'} dt' \quad (40)$$

which do not depend on perturbations to the carrier density, but only on the amplitude of the carrier grating. It is convenient to make the changes  $e_-(z, t) = a_-(z, t) e^{-i k_s z - i \omega_s t}$ ,  $p_-(z, t) = b_-(z, t) e^{-i k_s z - i \omega_s t}$ , and  $n_{-2}(z, t) = c_{-2}(z, t) e^{-2 i k_s z}$  which leads to

$$\partial_t a_- - \partial_z a_- = -i \tilde{\chi}_s a_- + i b_-, \quad (41)$$

$$\partial_t c_{-2} = -[R'(N_0^s) + \eta] c_{-2} - i(b_- E_+^{s*} - a_- P_+^{s*}), \quad (42)$$

$$b_-(z, t) = \int_0^{\infty} [\chi(t', N_0^s) a_-(z, t - t') + \chi_N(t', N_0^s) E_+^s c_{-2}(z, t - t')] dt', \quad (43)$$

where we have used Eq. 27. Assuming a perturbation that corresponds to a cavity mode (i.e., which spatial dependence is of the form  $e^{i k_{\ell} z}$  with  $k_{\ell} = 2\pi\ell$ ) the boundary conditions are

automatically satisfied. Introducing the eigenvalue  $\lambda$  for the temporal evolution, i.e.,

$$a_- = a_\ell^- e^{\lambda t} e^{-ik_\ell z}, \quad (44)$$

$$b_- = b_\ell^- e^{\lambda t} e^{-ik_\ell z}, \quad (45)$$

$$n_{-2} = \gamma_\ell e^{\lambda t} e^{-ik_\ell z}, \quad (46)$$

one arrives at the equation for the eigenvalues  $\lambda$ ,

$$\lambda + ik_\ell = i(\tilde{\chi}_\lambda - \tilde{\chi}_s) + \frac{\partial_N \tilde{\chi}_\lambda (\tilde{\chi}_\lambda - \tilde{\chi}_s^*) |E_+^s|^2}{R'(N_0^s) + \eta + i\partial_N \tilde{\chi}_\lambda |E_+^s|^2 + \lambda}, \quad (47)$$

where

$$\tilde{\chi}_\lambda = \int_0^\infty \chi(t', N_0^s) e^{i(\omega_s + i\lambda)t'} dt', \quad (48)$$

$$\partial_N \tilde{\chi}_\lambda = \int_0^\infty \partial_N \chi(t', N_0^s) e^{i(\omega_s + i\lambda)t'} dt'. \quad (49)$$

The eigenvalue equation for the counter-propagating perturbations can not be analytically solved due to the complicated dependence of  $\tilde{\chi}_\lambda$  and  $\partial_N \tilde{\chi}_\lambda$  on  $\lambda$ , which describe the spectral dependence of the optical response of the QW material and its variation with carrier density, respectively. These magnitudes, however, vary on wavelength intervals typically much larger than the characteristic mode spacing, hence one can expect the eigenvalue  $\lambda$  to be close to the modal frequency for mode  $\ell$ . Hence, defining  $\lambda = \lambda' - 2i\pi\ell$ —where  $\lambda'$  is small— and neglecting the effect of  $\lambda'$  in (48) and (49) allows to rewrite Eq. (47) as

$$\lambda' = i(\tilde{\chi}_\ell - \tilde{\chi}_s) + \frac{\partial_N \tilde{\chi}_\ell (\tilde{\chi}_\ell - \tilde{\chi}_s^*) |E_+^s|^2}{R'(N_0^s) + \eta + i\partial_N \tilde{\chi}_\ell |E_+^s|^2 + \lambda' - 2i\pi\ell}, \quad (50)$$

which is a second order polynomial in  $\lambda'$  quoted in the main text as Eq. (14) and where we have defined

$$\tilde{\chi}_\ell = \int_0^\infty \chi(t', N_0^s) e^{i(\omega_s + 2\pi\ell)t'} dt', \quad (51)$$

$$\partial_N \tilde{\chi}_\ell = \int_0^\infty \partial_N \chi(t', N_0^s) e^{i(\omega_s + 2\pi\ell)t'} dt'. \quad (52)$$

## B.2.2 Co-propagating perturbations

As discussed before, co-propagating perturbations evolve according to

$$\partial_t e_+ + \partial_z e_+ = ip_+ - \alpha_i e_+, \quad (53)$$

$$\partial_t n_0 = -R'(N_0^s) n_0 - i(P_+^s e^{i\Phi_s(z,t)} e_+^* + p_+ E_+^{s*} e^{-i\Phi_s(z,t)} - c.c.), \quad (54)$$

$$p_+(z, t) = \int_0^\infty [\chi(t', N_0^s) e_+(z, r) + \chi_N(t', N_0^s) E_+^s n_0(z, r) e^{i\Phi_s(z,r)}]_{r=t-t'} dt'. \quad (55)$$

Now, coupling of the field perturbations to the material occurs through the perturbations in the local carrier density, and the amplitude of the carrier grating does not play any role. This simply

reflects that co-propagating waves do not generate a carrier grating, but they simply create a modulation of the carrier density on long spatial distances as compared to the wavelength due to their beating. Please note that the above equations generalize the so-called relaxation oscillations to a spatially extended system.

It is convenient to pass to the reference frame of the UNI solution by setting  $e_+(z, t) = a_+(z, t)e^{i\Phi_s(z, t)}$ ,  $p_+(z, t) = b_+(z, t)e^{i\Phi_s(z, t)}$  which leads to

$$\partial_t a_+ + \partial_z a_+ = (i\omega_s - ik_s - \alpha_i)a_+ + ib_+, \quad (56)$$

$$\partial_t n_0 = -R'(N_0^s)n_0 - i(P_+^s a_+^* + b_+ E_+^{s*} - c.c.), \quad (57)$$

$$b_+ = \chi_0 \int_0^\infty e^{i\omega_s t'} [\chi(t', N_0^s)a_+(z, r) + \chi_N(t', N_0^s)n_0(z, r)E_+^s] dt', \quad (58)$$

together with the corresponding equations for  $a_+^*$  and  $b_+^*$ .

It is worth remarking that in these equations, perturbations can not be on a single mode only: disturbances  $\ell$  modes above the monochromatic solution are tied to perturbations  $\ell$  modes below via FWM mediated by the carrier density perturbation [45]. Therefore both have to be taken into account, for the sake of simplicity in the notation we suppose  $s = 0$ , hence we take

$$a_+ = a_{-\ell}(t)e^{-ik_\ell z} + a_\ell(t)e^{ik_\ell z}, \quad (59)$$

$$b_+ = b_{-\ell}(t)e^{-ik_\ell z} + b_\ell(t)e^{ik_\ell z}, \quad (60)$$

$$n_0 = c_{-\ell}(t)e^{-2ik_\ell z} + c_\ell(t)e^{2ik_\ell z}, \quad (61)$$

which yields

$$\partial_t a_{-\ell} = (2i\pi\ell + i\omega_s - ik_s - \alpha_i)a_{-\ell} + ib_{-\ell}, \quad (62)$$

$$\partial_t a_\ell = (-2i\pi\ell + i\omega_s - ik_s - \alpha_i)a_\ell + ib_\ell, \quad (63)$$

$$\partial_t c_{-\ell} = -R'(N_0^s)c_{-\ell} - i(P_+^s a_\ell^* + b_{-\ell} E_+^{s*} - P_+^{s*} a_{-\ell} - b_\ell^* E_+^s), \quad (64)$$

$$\partial_t c_\ell = -R'(N_0^s)c_\ell - i(P_+^s a_{-\ell}^* + b_\ell E_+^{s*} - P_+^{s*} a_m - b_{-\ell}^* E_+^s), \quad (65)$$

and

$$b_{-\ell} = \int_0^\infty e^{i\omega_s t'} [\chi(t', N_0^s)a_{-\ell}(t-t') + \chi_N(t', N_0^s)c_{-\ell}(t-t')E_+^s] dt', \quad (66)$$

$$b_\ell = \int_0^\infty e^{i\omega_s t'} [\chi(t', N_0^s)a_\ell(t-t') + \chi_N(t', N_0^s)c_\ell(t-t')E_+^s] dt'. \quad (67)$$

Clearly,  $c_{-\ell} = c_\ell^*$ , as expected since  $n_0$  is real. Introducing the eigenvalue  $\lambda$  as before and solving for the resulting system leads to

$$\begin{aligned} & \left[ \lambda - 2i\pi\ell - i(\tilde{\chi}_\lambda - \tilde{\chi}_s) - \frac{\partial_N \tilde{\chi}_\lambda (\tilde{\chi}_\lambda - \tilde{\chi}_s^*) |E_+^s|^2}{\lambda + Y_\lambda} \right] \\ & \times \left[ \lambda - 2i\pi\ell + i(\hat{\chi}_\lambda - \tilde{\chi}_s^*) - \frac{\partial_N \hat{\chi}_\lambda (\hat{\chi}_\lambda - \tilde{\chi}_s) |E_+^s|^2}{\lambda + Y_\lambda} \right] \\ & - \frac{\partial_N \tilde{\chi}_\lambda \partial_N \hat{\chi}_\lambda (\hat{\chi}_\lambda - \tilde{\chi}_s) (\tilde{\chi}_\lambda - \tilde{\chi}_s^*) |E_+^s|^4}{(\lambda + Y_\lambda)^2} = 0, \end{aligned} \quad (68)$$

where  $Y_\lambda = R'(N_0^s) - i(\partial_N \widehat{\chi}_\lambda - \partial_N \widetilde{\chi}_\lambda) |A_s|^2$ ,

$$\widetilde{\chi}_\lambda = \chi_0 \int_0^\infty \chi(t', N_0^s) e^{i(\omega_s + i\lambda)t'} dt', \quad (69)$$

$$\partial_N \widetilde{\chi}_\lambda = \chi_0 \int_0^\infty \partial_N \chi(t', N_0^s) e^{i(\omega_s + i\lambda)t'} dt', \quad (70)$$

$$\widehat{\chi}_\lambda = \chi_0 \int_0^\infty \chi^*(t', N_0^s) e^{-i(\omega_s - i\lambda)t'} dt', \quad (71)$$

$$\partial_N \widehat{\chi}_\lambda = \chi_0 \int_0^\infty \partial_N \chi^*(t', N_0^s) e^{-i(\omega_s - i\lambda)t'} dt', \quad (72)$$

and we have used (27) and that  $P_+^s = \widetilde{\chi}_s E_+^s$ .

As in the previous subsection, the eigenvalue must be close to the modal frequency, so we define  $\lambda = \lambda' - 2i\pi\ell$  and we approximate

$$\widetilde{\chi}_\lambda \simeq \chi_0 \int_0^\infty \chi(t', N_0^s) e^{i(\omega_s - 2\pi\ell)t'} dt' \equiv \widetilde{\chi}_{-\ell}, \quad (73)$$

$$\widehat{\chi}_\lambda \simeq \chi_0 \int_0^\infty \chi^*(t', N_0^s) e^{-i(\omega_s + 2\pi\ell)t'} dt' \equiv \widetilde{\chi}_\ell^*, \quad (74)$$

and accordingly for their derivatives with respect to carrier density. Hence we finally obtain the approximate eigenvalue equation

$$\begin{aligned} & \left[ \lambda' - i(\widetilde{\chi}_{-\ell} - \widetilde{\chi}_s) - \frac{\partial_N \widetilde{\chi}_{-\ell} (\widetilde{\chi}_{-\ell} - \widetilde{\chi}_s^*) |E_+^s|^2}{\lambda' + Y_\ell} \right] \\ & \times \left[ \lambda' + i(\widetilde{\chi}_\ell^* - \widetilde{\chi}_s^*) - \frac{\partial_N \widetilde{\chi}_\ell^* (\widetilde{\chi}_\ell^* - \widetilde{\chi}_s) |E_+^s|^2}{\lambda' + Y_\ell} \right] \\ & - \frac{\partial_N \widetilde{\chi}_{-\ell} \partial_N \widetilde{\chi}_\ell^* (\widetilde{\chi}_\ell^* - \widetilde{\chi}_s) (\widetilde{\chi}_{-\ell} - \widetilde{\chi}_s^*) |E_+^s|^4}{(\lambda' + Y_\ell)^2} = 0, \end{aligned} \quad (75)$$

where  $Y_\ell = 2i\pi\ell + R'(N_0^s) - i(\partial_N \widetilde{\chi}_\ell^* - \partial_N \widetilde{\chi}_{-\ell}) |E_+^s|^2$ . In this case Eq. (75) is a fourth order polynomial in  $\lambda'$  and it is given in the main text as Eq. (15).

## References

- [1] S. Yu and B. Li, "All-optical signal processing functions using semiconductor ring lasers", *Conference on Lasers and Electro-Optics Europe (CLEO EUROPE/EQEC) and 12th European Quantum Electronics Conference*, May 2011.
- [2] M. Sorel, G. Giuliani, A. Scirè, R. Miglierina, S. Donati and P. J. R. Laybourn, "Operating regimes of GaAs-AlGaAs semiconductor ring lasers: experiment and model", *IEEE J. Quantum Electron.*, vol. 39, no. 10, pp. 1187–1195, Oct. 2003.

- [3] M. Sorel, P. J. R. Laybourn, A. Scirè, S. Balle, G. Giuliani, R. Miglierina and S. Donati, “Alternate oscillations in semiconductor ring lasers”, *Opt. Lett.*, vol. 27, no. 22, pp. 1992–1994, 2002.
- [4] M. Sorel, P. J. R. Laybourn, G. Giuliani and S. Donati, “Unidirectional bistability in semiconductor waveguide ring lasers”, *Appl. Phys. Lett.*, vol. 80, no. 17, pp. 3051–3053, Apr. 2002.
- [5] L. Gelens, S. Beri, G. Van der Sande, G. Mezosi, M. Sorel, J. Danckaert and G. Verschaffelt, “Exploring multistability in semiconductor ring lasers: Theory and experiment”, *Phys. Rev. Lett.*, vol. 102, no. 19, p. 193904, May 2009.
- [6] S. Furst and M. Sorel, “Cavity-enhanced four-wave mixing in semiconductor ring lasers”, *IEEE Photon. Technol. Lett.*, vol. 20, no. 5, pp. 366–368, March 2008.
- [7] J. Javaloyes, A. Trita, G. Mezosi, F. Bragheri, I. Cristiani, G. Giuliani, M. Sorel, A. Scirè and S. Balle, “Ultrafast all-optical switching of bistable semiconductor ring lasers”, *Conference on Lasers and Electro-Optics Europe (CLEO EUROPE/EQEC) and 11th European Quantum Electronics Conference*, Jun. 2009.
- [8] Z. Wang, G. Yuan, X. Cai, G. Verschaffelt, J. Danckaert, Y. Liu and S. Yu, “Error-free 10-Gb/s all-optical switching based on a bidirectional SRL with miniaturized retro-reflector cavity”, *IEEE Photon. Technol. Lett.*, vol. 22, no. 24, pp. 1805–1807, Dec. 2010.
- [9] J. Sakaguchi, T. Katayama and H. Kawaguchi, “High switching-speed operation of optical memory based on polarization bistable vertical-cavity surface-emitting laser”, *IEEE J. Quantum Electron.*, vol. 46, no. 11, pp. 1526–1534, Nov. 2010.
- [10] M. T. Hill, H. J. S. Dorren, T. de Vries, X. J. M. Leijtens, J. H. den Besten, B. Smalbrugge, Y. S. Oei, H. Binsma, G. D. Khoe and M. K. Smit, “A fast low-power optical memory based on coupled micro-ring lasers”, *Nature*, vol. 432, no. 7014, pp. 206–209, Nov. 2004.
- [11] B. Li, M. Memon, G. Mezosi, Z. Wang, M. Sorel and S. Yu, “All-optical digital logic gates using bistable semiconductor ring lasers”, *J. Opt. Commun.*, vol. 30, p. 190, 2009.
- [12] A. Trita, G. Mezosi, M. Latorre-Vidal, M. Zanola, M. Strain, F. Bragheri, M. Sorel and G. Giuliani, “All-optical directional switching in bistable semiconductor-ring lasers”, *IEEE J. Quantum Electron.*, vol. 49, no. 10, pp.877–885, Oct. 2013.
- [13] S. Sunada, T. Harayama, K. Arai, K. Yoshimura, K. Tsuzuki, A. Uchida and P. Davis, “Random optical pulse generation with bistable semiconductor ring lasers”, *Opt. Express*, vol. 19, no. 8, pp. 7439–7450, Apr. 2011.
- [14] R. M. Nguimdo, G. Verschaffelt, J. Danckaert, X. Leijtens, J. Bolk and G. V. der Sande, “Fast random bit generation based on a single chaotic semiconductor ring laser”, *Opt. Express*, vol. 20, no. 27, pp. 28603–28613, Dec. 2012.
- [15] K. Thakulsukanant, B. Li, T. Memon, G. Mezosi, Z. Wang, M. Sorel and S. Yu, “All-optical label swapping using bistable semiconductor ring laser in an optical switching node”, *J. Lightwave Techn.*, vol. 27, no. 6, pp. 631–638, March 2009.

- [16] C. Born, M. Sorel and S. Yu, "Linear and nonlinear mode interactions in a semiconductor ring laser", *IEEE J. Quantum Electron.*, vol. 41, no. 3, pp. 261–271, March 2005.
- [17] I. Ermakov, S. Beri, M. Ashour, J. Danckaert, B. Docter, J. Bolk, X. Leijtens and G. Verschaffelt, "Semiconductor ring laser with on-chip filtered optical feedback for discrete wavelength tuning", *IEEE J. Quantum Electron.*, vol. 48, no. 2, pp. 129–136, Feb. 2012.
- [18] Z. Wang, G. Yuan, G. Verschaffelt, J. Danckaert and S. Yu, "Storing 2 bits of information in a novel single semiconductor microring laser memory cell", *IEEE Photon. Technol. Lett.*, vol. 20, no. 14, pp. 1228–1230, Jul. 2008.
- [19] S. Balle, "Simple analytical approximations for the gain and refractive index spectra in quantum-well lasers", *Phys. Rev. A*, vol. 57, no. 2, pp. 1304–1312, Feb. 1998.
- [20] S. Balle, "Analytical description of spectral hole-burning effects in active semiconductors", *Opt. Lett.*, vol. 27, no. 21, pp. 1923–1925, 2002.
- [21] J. Javaloyes and S. Balle, "Quasiequilibrium time-domain susceptibility of semiconductor quantum wells", *Phys. Rev. A*, vol. 81, no. 6, p. 062505, Jun. 2010.
- [22] J. Javaloyes and S. Balle, "Emission directionality of semiconductor ring lasers: A traveling-wave description", *IEEE J. Quantum Electron.*, vol. 45, no. 5, pp. 431–438, May 2009.
- [23] S. Fürst, A. Pérez-Serrano, A. Scirè, M. Sorel and S. Balle, "Modal structure, directional and wavelength jumps of integrated semiconductor ring lasers: Experiment and theory", *Appl. Phys. Lett.*, vol. 93, no. 25, p. 251109, 2008.
- [24] J. Javaloyes and S. Balle, "All-optical directional switching of bistable semiconductor ring lasers", *IEEE J. Quantum Electron.*, vol. 47, no. 8, pp. 1078–1085, Aug. 2011.
- [25] A. Pérez-Serrano, J. Javaloyes and S. Balle, "Multichannel wavelength conversion using four-wave mixing in semiconductor ring lasers", *IEEE Photon. Technol. Lett.*, vol. 25, no. 5, pp. 476–479, March 2013.
- [26] A. M. Yacomotti, L. Furfaro, X. Hachair, F. Pedaci, M. Giudici, J. R. Tredicce, J. Javaloyes, S. Balle, E. A. Viktorov and P. Mandel, "Dynamics of multimode semiconductor lasers", *Phys. Rev. A*, vol. 69, no. 5, p. 053816, May 2004.
- [27] M. Ahmed and M. Yamada, "Influence of instantaneous mode competition on the dynamics of semiconductor lasers", *IEEE J. Quantum Electron.*, vol. 38, no. 6, pp. 682–693, Aug. 2002.
- [28] A. Pérez-Serrano, J. Javaloyes and S. Balle, "Longitudinal mode multistability in ring and Fabry-Pérot lasers: the effect of spatial hole burning", *Opt. Express*, vol. 19, no. 4, pp. 3284–3289, Feb. 2011.
- [29] A. P. Bogatov, P. G. Eliseev and B. N. Sverdlov, "Anomalous interaction of spectral modes in a semiconductor laser", *IEEE J. Quantum Electron.*, vol. 11, no. 7, pp. 510–515, Jul. 1975.

- [30] L. M. Narducci and N. B. Abraham, *Laser physics and laser instabilities*, World Scientific Publishing, Singapore, 1988.
- [31] J. Javaloyes, M. Perrin, G. L. Lippi and A. Politi, "Self-generated cooperative light emission induced by atomic recoil", *Phys. Rev. A*, vol. 70, no. 2, p. 023405, Aug. 2004.
- [32] J. Javaloyes, M. Perrin and A. Politi, "Collective atomic recoil laser as a synchronization transition", *Phys. Rev. E*, vol. 78, no. 1, p. 011108, Jul. 2008.
- [33] G. L. Gattobigio, F. Michaud, J. Javaloyes, J. W. R. Tabosa and R. Kaiser, "Bunching-induced asymmetry in degenerate four-wave mixing with cold atoms", *Phys. Rev. A*, vol. 74, no. 4, p. 043407, Oct. 2006.
- [34] J. Javaloyes and S. Balle, "Detuning and thermal effects on the dynamics of passively mode-locked quantum-well lasers", *IEEE J. Quantum Electron.*, vol. 48, no. 12, pp. 1519–1526, Dec. 2012.
- [35] J. Javaloyes and S. Balle, "Multimode dynamics in bidirectional laser cavities by folding space into time delay", *Opt. Express*, vol. 20, no. 8, pp. 8496–8502, Apr. 2012.
- [36] J. Javaloyes and S. Balle, "Freetwm: a simulation tool for semiconductor lasers", <http://onl.uib.es/es/Softwares/Freetwm/>
- [37] A. Pérez-Serrano, J. Javaloyes and S. Balle, "Bichromatic emission and multimode dynamics in bidirectional ring lasers", *Phys. Rev. A*, vol. 81, no. 4, p. 043817, Apr. 2010.
- [38] O. Conradi, S. Helfert and R. Pregla, "Comprehensive modeling of vertical-cavity laser-diodes by the method of lines", *IEEE J. Quantum Electron.*, vol. 37, no. 7, pp. 928–935, Jul. 2001.
- [39] E. Doedel, A. R. Champneys, T. F. Fairgrieve, Y. A. Kuznetsov, B. Sandstede and X. Wang, "Auto: Software for continuation and bifurcation problems in ordinary differential equations", <http://indy.cs.concordia.ca/auto/>
- [40] K. Engelborghs, T. Luzyanina, G. Samaey, D. Roose and K. Verheyden, "DDE-bifTool v.2.03: A Matlab package for bifurcation analysis of delay differential equations", <http://twr.cs.kuleuven.be/research/software/delay/ddebiftool.shtml>
- [41] R. LeVeque, *Finite difference methods for ordinary and partial differential equations: steady-state and time-dependent problems*, Society for Industrial and Applied Mathematics, Philadelphia, 2007.
- [42] W. Press, *Numerical recipes: The art of scientific computing*, Cambridge University Press, Cambridge, 2007.
- [43] H. Risken and K. Nummedal, "Self-pulsing in lasers", *J. Appl. Phys.*, vol. 39, no. 10, pp. 4662–4672, 1968.

- [44] L. M. Narducci, J. R. Tredicce, L. A. Lugiato, N. B. Abraham and D. K. Bandy, "Mode-mode competition and unstable behavior in a homogeneously broadened ring laser", *Phys. Rev. A*, vol. 33, no. 3, pp. 1842–1854, March 1986.
- [45] L. A. Lugiato, L. M. Narducci and M. F. Squicciarini, "Exact linear stability analysis of the plane-wave Maxwell-Bloch equations for a ring laser", *Phys. Rev. A*, vol. 34, no. 4, pp. 3101–3108, Oct. 1986
- [46] L. Gelens, G. Van der Sande, S. Beri and J. Danckaert, "Phase-space approach to directional switching in semiconductor ring lasers", *Phys. Rev. E*, vol. 79, no. 1, p. 016213, Jan. 2009.
- [47] P. Mandel and G. P. Agrawal, "Mode instabilities in a homogeneously broadened ring laser", *Opt. Commun.*, vol. 42, no.4, pp. 269–274, July 1982.
- [48] M. Sargent III, "Theory of a multimode quasiequilibrium semiconductor laser", *Phys. Rev. A*, vol. 48, no. 1, pp.717–726, July 1993.